Published in final edited form as:
J Magn Reson Imaging. 2013 March ; 37(3): 717–726. doi:10.1002/jmri.23851.

R2* Estimation using "In-Phase" Echoes in the Presence of Fat: The Effects of Complex Spectrum of Fat

Diego Hernando, PhD[1], **Jens-Peter Kühn, MD**[1,2], **Birger Mensel, MD**[2], **Henry Völzke, MD, PhD**[3], **Ralf Puls, MD**[2], **Norbert Hosten, MD, PhD**[2], and **Scott B. Reeder, MD, PhD**[1,4,5,6]

[1]Department of Radiology, University of Wisconsin, Madison, WI, USA

[2]Department of Radiology and Neuroradiology, Ernst Moritz Arndt University Greifswald, Greifswald, Germany

[3]Institute for Community Medicine, Ernst Moritz Arndt University Greifswald, Greifswald, Germany

[4]Department of Medical Physics, University of Wisconsin, Madison, WI, USA

[5]Department of Biomedical Engineering, University of Wisconsin, Madison, WI, USA

[6]Department of Medicine, University of Wisconsin, Madison, WI, USA

Abstract

Purpose—To investigate R2* mapping robustness in the presence of fat using in-phase echoes, without and with spectral modeling of fat (single-peak and multi-peak models, respectively), using varying numbers of echoes.

Materials and Methods—Data from 88 volunteers (men/women: 52/36, ages: 55.4±12.2) were randomly chosen according to MRI liver fat-fraction (%), and classified into 6 fat-fraction groups (1: 20 cases, 0–<10%; 2: 20 cases, 10–<20%; 3: 20 cases, 20–<30%; 4: 20 cases, 30–<40%; 5: 8 cases >40% liver fat; 6: subcutaneous fat from all cases). R2* maps obtained from 5 in-phase echoes (echo times: 4.8–23.8ms) were retrospectively reconstructed using single-peak and multi-peak fat modeling. R2* maps were also calculated using different numbers (2–5) of echoes.

Results—Multi-peak fat corrected R2* mapping is feasible from in-phase echoes, with noise performance comparable to single-peak R2* when using ≥4 echoes. Single-peak R2* showed poor robustness to varying echo time combinations in the presence of fat, where using few echoes resulted in large errors. These errors can be reduced using more echoes, or fully corrected using multi-peak fat modeling. The mean R2* increased significantly with increasing fat-fraction when using single-peak R2* for any TE combination ($p<0.001$), but did not vary when using multi-peak R2* for any TE combination ($p\geq0.158$).

Conclusion—R2* mapping uncorrected for spectral complexity of fat contains protocol and fat-dependent errors (lack of robustness) in tissues with high fat content. Accounting for complex fat spectrum improves robustness and accuracy of signal fitting, with modest noise performance loss.

Keywords

R2*; liver; in-phase; fat; multi-peak

Contact Information: Diego Hernando, Ph.D, Department of Radiology, University of Wisconsin, 1111 Highland Ave, Madison, WI 53705, USA, dhernando@wisc.edu, Tel: 001 (608) 265-7590.

Author contribution statement:
'Diego Hernando, PhD and Jens-Peter Kühn, MD contributed equally to this work'

Introduction

R2* mapping, based on quantifying the relaxation rate R2*=1/T2*, has multiple applications in MRI, including the assessment of blood oxygenation (1,2), detection of super-paramagnetic iron oxides (3), and the measurement of tissue iron levels (4–7). R2* mapping is typically performed by acquiring a sequence of gradient-echo images with increasing echo times (TEs), and measuring the temporal relaxation rate of the signal at each voxel.

It has long been recognized that R2* mapping is complicated by the presence of tissue fat (8–11). The fat MR signal contains multiple resonances, with its main peak (CH2) approximately 3.3 ppm away from the water peak (i.e., approximately −217 Hz at 1.5T). The main CH2 fat peak arises from the protons in the methylene moiety in triglycerides and fatty acids, and accounts for approximately 70% of the total fat proton signal (14). MR signal originating from fat also has several smaller fat peaks at various frequencies relative to the water (10,12–15). As a result of these multiple fat resonances, the MR signal contains complex oscillations arising from the temporal evolution of the relative phase between the different contributing peaks. If not accounted for, these oscillations will result in large errors in R2* mapping techniques. Furthermore, these errors will be dependent on the specific TE combination, i.e., will reduce the robustness of R2* mapping to changes in the acquisition parameters.

A simple approach that is commonly used to avoid the effects of fat is to acquire so-called “in-phase” echoes (IP). In this technique, the fat signal is approximated as a single resonance (e.g., −217 Hz at 1.5T), and TEs are chosen such that the main fat peak is in-phase with the water signal (e.g., at 1.5T: 4.7ms, 9.4ms, 14.1ms, etc). Thus, in locations containing both water and fat, the MR signal will be measured near the maximum of each oscillation. R2* maps are simply obtained by fitting a decaying exponential (with decay rate R2*) to the measured signal at these IP TEs. IP acquisitions are often used in practice for R2* mapping (3,16). However, the effectiveness of this technique is based on the underlying (and incorrect) assumption of a “single-peak” fat signal, as the fat spectrum is truly “multi-peak” (spectral complexity of the fat signal). Smaller fat peaks, which are generally not in-phase with water at the IP TEs, account for approximately 30% of the fat signal. Specifically, these smaller fat peaks may affect the accuracy and robustness of IP R2* mapping (17), although these effects have not been thoroughly assessed (11,18).

In principle, the effects of the spectral complexity of fat can be compensated by using a large number of IP echoes for R2* estimation or can be corrected by accounting for the spectral complexity of the fat signal in the estimation of R2* maps (i.e., multi-peak fat-corrected R2* mapping) **(**Figure 1**)** (11). Therefore, the purpose of this study was to investigate the robustness of R2* mapping techniques using different number of IP echoes and multi-spectral fat correction in subjects with varying levels of liver fat.

Material and Methods

Theory

In a gradient echo acquisition, the signal magnitude measured at a given voxel, at echo time TE_n (n=1,2,3,4,5 in this work), in the presence of water and fat signals and R2* decay can be described as:

$$S_n\left(\rho_W,\rho_F,R_2^*\right)=e^{-R_2^*TE_n}\left|\rho_W+\rho_F\sum_{p=1}^{P}\alpha_p e^{i2\pi f_{F,p}TE_n}\right| \quad [1]$$

where ρ_W and ρ_F are the amplitudes of water and fat signals, respectively, R2*=1/T2*, $f_{F,p}$ are the known frequencies for the multiple spectral peaks of the fat signal relative to the water peak, α_p are the relative amplitudes of the fat signal such that $\sum_{p=1}^{P}\alpha_p=1$ (10,11). The values of α_p and $f_{F,p}$ are are based on measurements made in 121 patients with hepatic steatosis by Hamilton et al (14), and are assumed fixed in this work. This assumption has been shown to be accurate in previous works (14,19,20) With fixed $f_{F,p}$ and α_p, the signal model in Eq. (1) has three unknown parameters (ρ_W, ρ_F and R2*). I

In general (and due to the multi-peak nature of the fat signal), the unknown quantities ρ_W, ρ_F and R2* will affect the measured signal, even if IP echoes are acquired, because the smaller fat peaks will not be in-phase with the water signal. In this work, these three unknowns will be estimated using nonlinear least-squares fitting (21) of the signal model (Eq. [1]) to the magnitude of the acquired signal. In this way, the resulting estimates of R2* are corrected for the multi-peak fat signal. Because there are three unknown parameters (ρ_W, ρ_F and R2*) multi-peak based R2* measurements can be performed using ≥ 3 echoes.

To test the IP approximation, R2* maps were also reconstructed using a single-peak fat model. In this model, the fat signal is approximated by a single peak (P=1, $\alpha_1=1$ and $f_{F,1}\approx -217$ Hz in Eq. 1), and since the IP TEs are $TE_n = n/f_{F,1}$, the signal model reduces to:

$$S_n\left(\rho_W,\rho_F,R_2^*\right)=e^{-R_2^*TE_n}\left|\rho_W+\rho_F e^{i2\pi f_{F,p}TE_n}\right| \quad [2]$$

$$S_n\left(\rho_W,\rho_F,R_2^*\right)=e^{-R_2^*TE_n}\left|\rho_W+\rho_F e^{i2\pi n}\right| \quad [3]$$

$$S_n\left(\rho_W+\rho_F,R_2^*\right)=e^{-R_2^*TE_n}\left|\rho_W+\rho_F\right| \quad [4]$$

where the contributions of water and fat cannot be separated from each other, and R2* can be estimated by a simple exponential fitting for the total signal amplitude $\rho_W+\rho_F$, and the R2* decay. In this work, this fitting is also performed using nonlinear least-squares (21). Note that, because there are only two unknown parameters, single-peak based R2* measurements can be performed using two or more echoes.

To test the robustness of R2* reconstructions to varying acquisition parameters, single-peak R2* reconstructions (which require at least two echoes, as described above) were performed using four different combinations of IP echoes: first two, first three, first four and all five echoes. Multi-peak R2* reconstructions (which require at least three echoes, as described above) were performed using three different echo combinations: first three, first four and all five echoes.

Simulations

A simulation study was performed to test the bias and noise performance of single-peak and multi-peak R2* reconstructions using the TE combinations described above. Complex-valued signals were simulated using R2*=45 s^{-1}, multi-peak (six peak) signal model (14) and a range of fat fractions from 0 to 100%, for the first five IP TEs. Complex Gaussian noise was added to the simulated signal, for a signal-to-noise ratio of 30 at TE=0. A total of 4096 instances of the noisy signal were created. For each instance, the signal magnitude was processed as described above (single-peak based R2* using two, three, four and five echoes, and multi-peak based R2* using three, four and five echoes). Finally, the mean and standard

deviation of single-peak and multi-peak R2* were computed for each echo combination and fat fraction.

Subjects

Healthy volunteers used in this study were retrospectively randomized according to their liver fat content from the ongoing population-based Study of Health in Pomerania (SHIP) at the University Medicine Greifswald.

SHIP is a population-based project conducted in Northeast Germany. The objectives of this interdisciplinary cohort study are to estimate the prevalence and incidence of risk factors and diseases and to investigate the complex associations among risk factors, subclinical disorders and diseases (22). Since 2008, whole body MRI has been part of SHIP, including three-echo complex chemical shift based MRI and a co-registered R2* mapping sequence using 5 IP echoes throughout the liver (23,24). All studies performed as part of SHIP were IRB approved, and informed consent was obtained from all subjects.

Liver fat quantification was performed using a 3D, three-echo-complex chemical shift MRI (out-phase, in-phase, in-phase imaging). Known confounding factors for liver fat quantification using complex chemical shift technique such as R2* bias, T1 bias, bias from multiple fat peaks, and noise bias were eliminated, and a calculation of the proton-density fat fraction (PDFF) was performed (10,11,25). PDFF is a standardized, objective MR-based measurement of an inherent tissue property (the ratio of MR-visible fat protons to the total MR-visible protons in tissue), and has the potential to provide a *platform-independent* biomarker unaffected by technical or biological variability (18). At this time, PDFF has been calculated for more than 2,303 SHIP volunteers, and 88 of them were randomly selected according to their liver fat content.

The 88 subjects consisted of 52 men, aged 52.0 ± 12.2 years and 36 women, aged 60.4 ± 10.6 years. Subjects were chosen to cover a wide range of liver fat-fraction, based on PDFF measurements: group 1: 20 subjects with a liver fat fraction of 0 – < 10%; group 2: 20 subjects with a liver fat-fraction of 10 – < 20%; group 3: 20 subjects with a liver fat-fraction of 20 – < 30%; group 4: 20 subjects with a liver fat-fraction of 30 – <40%; and group 5: 8 subjects with a liver fat content larger than 40%. The number of group 5 was limited because a PDFF > 40% was uncommon (only 8 of 2303 subjects fulfilled this criterion). In addition, measurement of subcutaneous fat tissue in all 88 subjects was performed to reflect very high fat content and was classified as group 6. Baseline characteristics of all subjects according to their liver fat content are listed in Table 1. R2* mapping from 88 subjects was reconstructed retrospectively from the magnitude source images.

MR Imaging and R2* Mapping

MR imaging was performed using a commercially available 1.5 Tesla MRI system (Magnetom Avanto, Siemens Healthcare, Erlangen, Germany). A 3D three-echo-complex chemical shift MRI (out-phase, in-phase, in-phase imaging) and a multi-echo 2D-GRE acquisition including 5 in-phase TEs (R2* mapping) was performed in one examination for each subject. The three-echo sequence included the following scan parameters: TR/TE_1/TE_2/TE_3=11/2.4/4.8/9.6 ms; flip angle = 10°; averages = 1; bandwidth = ±1065 Hz/pixel; matrix= 224 × 168 × 64, field of view = 410 × 308 mm, parallel imaging (GRAPPA) effective acceleration factor = 1.8), slice thickness = 3.0 mm. The five-echo R2* mapping sequence included the following scan parameters: TR: 168 ms; $TE_{1–5}$: 4.76 ms, 9.53 ms, 14.29 ms, 19.06 ms, 23.82 ms; flip angle = 25°; averages = 1; bandwidth = ±250Hz/pixel; matrix = 256 × 192; field of view = 450 × 337 mm; no parallel imaging; 6 slices with thickness = 5.0 mm and 15 mm gap between slices.

Data Analysis

One reader with over five years experience in hepatobiliary MR imaging measured the PDFF and R2* values from different data reconstructions: four based on single-peak fat modeling (using two, three, four and five echoes), and three based on multi-peak fat modeling (using three, four and five echoes).

In each subject, operator-defined regions of interest (ROI) based measurement of PDFF and R2*`s were performed in Couinaud's segment 6. Care was taken to avoid blood vessels and regions obviously contaminated by partial volume effects and/or motion artifacts when placing the ROI. An additional ROI was placed in the ventral subcutaneous fat tissue. The ROI size in the liver was 1.5–2.0cm^2 and was adjusted in each subject to fit within the subcutaneous fat tissue. For each ROI, the average and standard deviation of the R2* measurement, as well as the area of the ROI was recorded.

ROI placements were perfectly co-registered in each reconstruction using the copy and paste function of the measurement tool Osirix (version 3.9.1, Pixameo Sarl, Bernex, Switzerland).

Statistics

Differences between R2* values for each reconstruction (single-peak based R2* using two, three, four, and five echoes; and multi-peak based R2* using three, four, and five echoes) as a function of PDFF of liver tissue (groups 1–5) were calculated using the Kruskal Wallis test to test the influence of fat for each reconstruction. In addition, differences between R2* values for each fat group (group 1–6) as a function of the number of echoes for single-peak and multi-peak model were calculated using the Friedman test to assess the robustness of each method. Results were considered statistically significant for p values <0.05.

Further, confidence intervals (95%) of the paired differences between single-peak R2* measurements using different numbers of echoes (two vs. three, three vs. four, and four vs. five TEs), and multi-peak R2* measurements using different numbers of echoes (three vs. four, and four vs. five TEs), were calculated for each of the fat groups.

Finally, the mean of the R2* standard deviation from each case was measured as a metric of image noise.

Variables were described as mean values and standard deviations. Analyses and plots were performed using commercially available software (SPSS, release 14.0, Chicago, IL, USA and Matlab, R2011a, Mathworks, Natick, MA, USA).

Results

Simulated signals containing different levels of fat, along with their corresponding single-peak fits are shown in Figure 1. Note the increasing errors and decreasing robustness of single-peak R2* measurements at higher fat concentrations. A summary of the subject results is shown in Table 2. An example from one subject shown in Figure 2 demonstrates *in-vivo* R2* maps in the presence of fat using single-peak and multi-peak reconstruction with different in-phase echo combinations. The results from this subject are in excellent agreement with the theoretical results in Figure 1B (simulation of fat-fraction 40% and R2* of $45s^{-1}$).

Figure 3 shows a simulation of R2* measurements in the presence of fat without **(**Figure 3A**)** and with **(**Figure 3B**)** multi-peak fat modeling with increasing numbers of echoes used for the reconstruction. According to these simulations, single-peak fat modeling with a low number of echoes results in large R2* errors in the presence of fat. These errors can be

reduced by using more echoes or completely corrected by using multi-peak fat modeling. It should be noted, however, that multi-peak reconstructions from three TEs resulted in small fat-independent R2* errors, possibly due to instability in the presence of noise.

Subject results grouped by their liver fat content are illustrated in Figure 4. These results show an excellent agreement with the simulation in Figure 3. Using single-peak R2* reconstructions, the mean apparent R2* increased with increasing liver fat fraction for each TE-combination and resulted in significant differences in the presence of fat (differences in mean R2* according to the fat group 2–5 for each TE combination: $p \leq 0.001$). Using multi-peak reconstructions, there were no statistically significant differences between liver R2* values in groups of liver fat (group 2–5) when using three echoes (p=0.396), four echoes (p=0.291), or five echoes (p=0.158) **(**Figure 4**)**.

In the presence of fat, the mean R2* values for each fat group (shown in Table 2) were reduced using a single-peak reconstruction with a large number of echoes (differences in mean R2* according to the TE combination for each fat group 2–6: $p \leq 0.001$). Using multi-peak reconstruction there was also a significant difference in mean R2* as a function of the TE combination for each fat group 2,3,4,6: $p \leq 0.001$, but no statistical differences for fat group 5 (p=0.093).

Table 3 shows the 95% confidence intervals of the paired differences between reconstructions from different TE combinations, for each fat group. In the presence of fat, different TE combinations result in large differences in single-peak R2* measurements. These differences are smaller for multi-peak R2* measurements, and not caused by the fat content (likely due to higher noise using multi-peak reconstruction and small number of echoes).

Figure 5 compares the noise performance of single-peak and multi-peak R2* measurements using 2–5 IP echoes, and 3–5 echoes, respectively. R2* standard deviation is shown from simulations with single-peak **(**Figure 5A**)** and multi-peak fat modeling **(**Figure 5B**)** as well as for all subjects with single-peak **(**Figure 5C**)** and multi-peak fat modeling **(**Figure 5D**)**. The behavior of the R2* noise performance for simulations and from subjects are comparable. For the simulations in this Figure, it was assumed the liver R2* was 45 s^{-1}. In practice (subjects) it should be noted that group six consists of mostly fat, and the baseline R2* values are fundamentally different from liver R2*, independent of reconstruction type and number of echoes. In addition, the signal-to-noise ratio (SNR) in the subcutaneous fat was higher than in the liver, due to the use of surface coils, which leads to lower standard deviation in the subcutaneous fat R2* measurements. Simulation and subject data show clearly that the noise performance can be improved using more echoes for both reconstructions. Noise performance was comparable for single-peak and multi-peak reconstructions when using four or more echoes. Multi-peak fat reconstructions from three echoes resulted in severely increased noise in R2* maps.

Discussion

R2*-MRI is complicated by the presence of fat in tissues. Fat introduces oscillations in the acquired signal, resulting in systematic errors in R2* measurements, unless the presence of fat is accounted for. A common strategy is to acquire “in-phase” echoes, where the TEs are chosen such that the main methylene peak of fat is always in-phase with water signal. R2* measurements from IP echoes are typically performed by modeling the magnitude of the acquired signal as a decaying exponential; an inherent assumption of this approach is that fat has a single-peak fat model. However, fat signal contains multiple spectral peaks in addition to the main methylene peak, which lead to complex oscillations that are not accounted for by

"in-phase" echoes. For this reason, the term "in-phase" is actually a misnomer, since water and fat signals are never truly in-phase except at TE=0 or at a spin-echo.

In this work we have shown that R2* measurements made using in-phase echoes, when uncorrected for the spectral complexity of fat results in significant errors in the presence of fat. The degree of the error depends on the specific choice of TE combination, i.e., R2* mapping with in-phase echoes is not a robust method to quantify R2*. Furthermore, multi-peak fat corrected R2* measurement is possible, even using IP echoes. Multi-peak fat corrected R2* measurements are necessary to remove R2* errors in the presence of fat and improve the robustness of the R2* mapping relative to single-peak measurements.

R2* mapping is an important and clinically accepted non-invasive biomarker to quantify hepatic iron concentration (6). However, R2* measurements have varying sensitivities to quantify the cellular iron concentration in the presence of various liver diseases (5). Fatty liver disease is a common disease with a prevalence of approximately 20–30% (26–28). Further, an association between hepatic steatosis and liver iron overload has been demonstrated with up to 40% of patients with non-alcoholic fatty liver disease having concomitant iron overload (29–32). Our results show clearly that subjects with hepatic steatosis may be misdiagnosed for hepatic iron overload using single-peak reconstruction, depending on the number of IP echoes used for the reconstruction and depending on the amount of liver fat. Thus, it is necessary to use the multi-peak fat model in order to obtain accurate fat-independent R2* estimates.

As expected from theory, R2* errors in subjects using single-peak measurements decrease with increasing numbers of echoes - using a large number of echoes results in improved estimation of R2* in the presence of low and medium fatty tissue. Intuitively, this occurs because with increasing number of echoes, the complex oscillations and interactions of the multiple peaks of fat tend to average out **(**Figure 1**)**. For instance, for five IP echoes, R2* errors are small except for fat fractions >40% and subcutaneous fat. However, spectral modeling of fat can be performed from the same data as single-peak R2* measurements, producing robust R2* measurements regardless of the amount of fat, independently of the number of echoes, and with comparable noise performance to single-peak for four or more echoes. Therefore, it is preferable to always include multi-peak fat correction in tissues that may contain fat.

Furthermore, since IP echoes do not result in truly fat-corrected signals (and multi-peak fat modeling is necessary even with this choice of TEs), there are no advantages to acquiring IP echoes. Specifically, IP echoes are very widely spaced and are poor choices for measuring high R2* (e.g., liver iron overload). At high R2*, the signal decays very rapidly, leading to poor noise performance and limited dynamic range of R2* estimation from IP echoes. Much shorter echoes are necessary to estimate R2* accurately when R2* is high. Although not shown in this work, it is expected that multi-peak fat modeling can provide fat-corrected R2* measurements over a wide range of TE combinations (with varying initial TE and echo spacings). It is likely that the optimum TE combination for fat-corrected R2* measurement is generally dependent on the underlying true R2* value and can be used in combination with multi-peak fat-corrected R2* reconstruction.

An alternative approach to remove the effects of fat in R2* mapping is to suppress the fat signal during acquisition (33). This can be achieved using short-tau inversion recovery techniques (which seek to null the fat signal based on its T1 relaxivity) (34), or chemical shift based fat suppression techniques (fat saturation or spatial-spectral excitation techniques) (35,36). Although these techniques work well in some cases, they have fundamental limitations such as decreased signal to noise ratio, increased scan time, and

sensitivity to B0 and B1 inhomogeneities (37–39). Further, these approaches do not suppress all peaks of fat, particularly those fat peaks near the water peak, and a residual effect of unsuppressed fat peaks could lead to potential bias in the estimation of R2*. Additional work would need to be performed to determine the magnitude of this potential bias. Of note, the R2* values measured in this study are very comparable to those measured in 129 healthy subjects by Schwenzer et al, using a fat-saturated R2* estimation method (33). Note that multi-peak fat corrected reconstructions require no overhead in the acquisition (as opposed to, e.g., fat-saturation pulses), and therefore is the most efficient approach to avoid the effects of fat.

The proposed multi-peak fat-corrected R2* measurement technique is based on a "single-R2*" model, where the R2* relaxivities of water and fat are assumed to be similar at each voxel and are modelled as a common value (equation [1]). To the best of our knowledge, it is unknown whether this is the case for liver tissue in the presence of iron overload, although the single-R2* model has been shown to be accurate for fat quantification in the presence of iron in mice (40) and in phantoms when the size of the fat particles is similar to those in vivo (41). It must be noted that the single-R2* model is also an underlying assumption of conventional IP single-peak R2* reconstructions, and a single-R2 model is also an assumption of conventional R2 (=1/T2) based techniques.

The effects studied in this work likely occur also with different TE combinations (e.g., out-phase and in-phase acquisitions) if the spectral complexity of fat is not accounted for. These effects will also occur at different field strengths (eg. 3.0 T), although the magnitude of these effects may be different due to differences in the underlying R2* at different field strengths.

The main limitation of this study is the lack of ground truth for R2* measurements in subjects. However, our results clearly demonstrate that fat is a confounding factor for R2* quantification when fat is (incorrectly) modelled as a single-peak, because there is a strong dependence on the apparent R2* with increasing fat fraction and number of echoes.

This work included R2* measurements from liver as well as from subcutaneous fat. R2* values in liver are not expected to be the same as in subcutaneous fat. However, multi-peak fat modeling results in more robust R2* mapping in the subcutaneous fat. The multi-peak model of triglycerides used in this work has been derived and shown to be accurate for liver fat, and so it is unclear whether this model is as accurate for subcutaneous fat quantification. Although this model is likely more accurate than single-peak fat modeling, future work is needed to determine the optimal spectral model of triglycerides for fat and R2* quantification in adipose tissue.

Another limitation of this work is the lack of cases with very high liver R2* values (severe iron overload). The effect of the spectral complexity of the fat signal is unclear in these cases. However, in the presence of severe iron overload the liver signal decays very rapidly and in-phase echoes are likely too long to adequately capture this decay. This challenge may be overcome by acquiring short echoes and performing fat-corrected R2* mapping. Future work will be needed to validate this approach.

In conclusion, the spectral complexity of the fat signal is an important factor that leads to inaccurate estimation of R2*, even when "in-phase" echoes are acquired. Indeed, the spectral complexity of fat implies that there is no such entity as "in-phase" echo times, other than TE=0 or at a spin-echo. R2* measurements uncorrected for multi-peak fat contain protocol-dependent errors in tissues containing fat. Accounting for the spectral complexity of fat results in improved robustness in R2* mapping, and improved accuracy in fitting of the signal model, achieving comparable noise performance for 4 or more echoes.

Additionally, multi-peak corrected R2* measurements may eliminate the constraint for in-phase echoes, providing improved flexibility in the acquisition, leading to potential improvements in SNR performance and improved dynamic range for R2* estimation.

Acknowledgments

We acknowledge the use of the GNU Scientific Library (GSL) to perform the reconstructions described in this work. Further, we thank Alejandro Munoz-Del Rio for statistical discussions.

Funding/Support:

SHIP is part of the Community Medicine Research net of the University of Greifswald, Germany, which is funded by the Federal Ministry of Education and Research, the Ministry of Cultural Affairs as well as the Social Ministry of the Federal State of Mecklenburg-West Pomerania. Whole-body MR imaging including study sequences was supported by a joint grant from Siemens Healthcare, Erlangen, Germany and the Federal State of Mecklenburg-Vorpommern.

We acknowledge the support of the NIH (R01 DK083380, R01 DK088925 and RC1 EB010384), the Coulter Foundation, and the Wisconsin Alumni Research Foundation (WARF) Accelerator Program.

References

1. Ogawa S, Menon RS, Tank DW, Kim SG, Merkle H, Ellermann JM, et al. Functional brain mapping by blood oxygenation level-dependent contrast magnetic resonance imaging. A comparison of signal characteristics with a biophysical model. Biophys J. 1993; 64(3):803–812. [PubMed: 8386018]
2. Sadowski EA, Djamali A, Wentland AL, Muehrer R, Becker BN, Grist TM, et al. Blood oxygen level-dependent and perfusion magnetic resonance imaging: detecting differences in oxygen bioavailability and blood flow in transplanted kidneys. Magnetic Resonance Imaging. 2010; 28(1): 56–64. [PubMed: 19577402]
3. Dahnke H, Schaeffter T. Limits of detection of SPIO at 3.0 T using T2 relaxometry. Magn Reson Med. 2005; 53(5):1202–1206. [PubMed: 15844156]
4. Ordidge RJ, Gorell JM, Deniau JC, Knight RA, Helpern JA. Assessment of relative brain iron concentrations using T2-weighted and T2*-weighted MRI at 3 Tesla. Magn Reson Med. 1994; 32(3):335–341. [PubMed: 7984066]
5. Anderson LJ, Holden S, Davis B, Prescott E, Charrier CC, Bunce NH, et al. Cardiovascular T2-star (T2*) magnetic resonance for the early diagnosis of myocardial iron overload. Eur Heart J. 2001; 22(23):2171–2179. [PubMed: 11913479]
6. Wood JC. MRI R2 and R2* mapping accurately estimates hepatic iron concentration in transfusion-dependent thalassemia and sickle cell disease patients. Blood. 2005; 106(4):1460–1465. [PubMed: 15860670]
7. Hankins JS, McCarville MB, Loeffler RB, Smeltzer MP, Onciu M, Hoffer FA, et al. R2* magnetic resonance imaging of the liver in patients with iron overload. Blood. 2009; 113(20):4853–4855. [PubMed: 19264677]
8. Hilaire L, Wehrli FW, Song HK. High-speed spectroscopic imaging for cancellous bone marrow R(2)* mapping and lipid quantification. Magn Reson Imaging. 2000; 18(7):777–786. [PubMed: 11027870]
9. Wehrli FW, Ma J, Hopkins JA, Song HK. Measurement of R'2 in the presence of multiple spectral components using reference spectrum deconvolution. J Magn Reson. 1998; 131(1):61–68. [PubMed: 9533907]
10. Bydder M, Yokoo T, Hamilton G, Middleton MS, Chavez AD, Schwimmer JB, et al. Relaxation effects in the quantification of fat using gradient echo imaging. Magn Reson Imaging. 2008; 26(3): 347–359. [PubMed: 18093781]
11. Yu H, Shimakawa A, McKenzie CA, Brodsky E, Brittain JH, Reeder SB. Multiecho water-fat separation and simultaneous R2* estimation with multifrequency fat spectrum modeling. Magn Reson Med. 2008; 60(5):1122–1134. [PubMed: 18956464]

12. Szczepaniak LS, Babcock EE, Schick F, Dobbins RL, Garg A, Burns DK, et al. Measurement of intracellular triglyceride stores by H spectroscopy: validation in vivo. Am J Physiol. 1999; 276(5 Pt 1):E977–E989. [PubMed: 10329993]
13. Thomsen C, Becker U, Winkler K, Christoffersen P, Jensen M, Henriksen O. Quantification of liver fat using magnetic resonance spectroscopy. Magn Reson Imaging. 1994; 12(3):487–495. [PubMed: 8007779]
14. Hamilton G, Yokoo T, Bydder M, Cruite I, Schroeder ME, Sirlin CB, et al. In vivo characterization of the liver fat ^{1}H MR spectrum. NMR Biomed. 2011; 24(7):784–790. [PubMed: 21834002]
15. Ling M, Brauer M. Ethanol-induced fatty liver in the rat examined by in vivo 1H chemical shift selective magnetic resonance imaging and localized spectroscopic methods. Magn Reson Imaging. 1992; 10(4):663–677. [PubMed: 1501537]
16. Wehrli FW, Ford JC, Haddad JG. Osteoporosis: clinical assessment with quantitative MR imaging in diagnosis. Radiology. 1995; 196(3):631–641. [PubMed: 7644622]
17. Sirlin CB, Reeder SB. Magnetic resonance imaging quantification of liver iron. Magn Reson Imaging Clin N Am. 2010; 18(3):359–381. ix. [PubMed: 21094445]
18. Reeder SB, Sirlin CB. Quantification of liver fat with magnetic resonance imaging. Magn Reson Imaging Clin N Am. 2010; 18(3):337–357. ix. [PubMed: 21094444]
19. Hines CDG, Frydrychowicz A, Hamilton G, Tudorascu DL, Vigen KK, Yu H, et al. T(1) independent, T(2) (*) corrected chemical shift based fat-water separation with multi-peak fat spectral modeling is an accurate and precise measure of hepatic steatosis. J Magn Reson Imaging. 2011; 33(4):873–881. [PubMed: 21448952]
20. Meisamy S, Hines CDG, Hamilton G, Sirlin CB, McKenzie CA, Yu H, et al. Quantification of hepatic steatosis with T1-independent, T2-corrected MR imaging with spectral modeling of fat: blinded comparison with MR spectroscopy. Radiology. 2011; 258(3):767–775. [PubMed: 21248233]
21. Hernando D, Liang Z-P, Kellman P. Chemical shift-based water/fat separation: a comparison of signal models. Magn Reson Med. 2010; 64(3):811–822. [PubMed: 20593375]
22. Völzke H, Alte D, Schmidt CO, Radke D, Lorbeer R, Friedrich N, et al. Cohort profile: the study of health in Pomerania. Int J Epidemiol. 2011; 40(2):294–307. [PubMed: 20167617]
23. Hegenscheid K, Kühn J, Völzke H, Biffar R, Hosten N, Puls R. Whole-Body Magnetic Resonance Imaging of Healthy Volunteers: Pilot Study Results from the Population-Based SHIP Study. Fortschr Röntgenstr. 2009; 181(08):748–759.
24. Puls R, Hamm B, Hosten N. [MRI without radiologists--ethical aspects of population based studies with MRI imaging]. Fortschr Röntgenstr. 2010; 182(6):469–471.
25. Liu C-Y, McKenzie CA, Yu H, Brittain JH, Reeder SB. Fat quantification with IDEAL gradient echo imaging: correction of bias from T(1) and noise. Magn Reson Med. 2007; 58(2):354–364. [PubMed: 17654578]
26. Völzke H, Robinson DM, Kleine V, Deutscher R, Hoffmann W, Ludemann J, et al. Hepatic steatosis is associated with an increased risk of carotid atherosclerosis. World J Gastroenterol. 2005; 11(12):1848–1853. [PubMed: 15793879]
27. Boyce CJ, Pickhardt PJ, Kim DH, Taylor AJ, Winter TC, Bruce RJ, et al. Hepatic steatosis (fatty liver disease) in asymptomatic adults identified by unenhanced low-dose CT. AJR Am J Roentgenol. 2010; 194(3):623–628. [PubMed: 20173137]
28. Szczepaniak LS, Nurenberg P, Leonard D, Browning JD, Reingold JS, Grundy S, et al. Magnetic resonance spectroscopy to measure hepatic triglyceride content: prevalence of hepatic steatosis in the general population. Am J Physiol Endocrinol Metab. 2005; 288(2):E462–E468. [PubMed: 15339742]
29. Dongiovanni P, Fracanzani AL, Fargion S, Valenti L. Iron in fatty liver and in the metabolic syndrome: a promising therapeutic target. J Hepatol. 2011; 55(4):920–932. [PubMed: 21718726]
30. Bonkovsky HL, Jawaid Q, Tortorelli K, LeClair P, Cobb J, Lambrecht RW, et al. Non-alcoholic steatohepatitis and iron: increased prevalence of mutations of the HFE gene in non-alcoholic steatohepatitis. J Hepatol. 1999; 31(3):421–429. [PubMed: 10488699]

31. George DK, Goldwurm S, MacDonald GA, Cowley LL, Walker NI, Ward PJ, et al. Increased hepatic iron concentration in nonalcoholic steatohepatitis is associated with increased fibrosis. Gastroenterology. 1998; 114(2):311–318. [PubMed: 9453491]
32. Moirand R, Mortaji AM, Loréal O, Paillard F, Brissot P, Deugnier Y. A new syndrome of liver iron overload with normal transferrin saturation. Lancet. 1997; 349(9045):95–97. [PubMed: 8996422]
33. Schwenzer NF, Machann J, Haap MM, Martirosian P, Schraml C, Liebig G, et al. T2* relaxometry in liver, pancreas, and spleen in a healthy cohort of one hundred twenty-nine subjects-correlation with age, gender, and serum ferritin. Invest Radiol. 2008; 43(12):854–860. [PubMed: 19002057]
34. Bydder GM, Steiner RE, Blumgart LH, Khenia S, Young IR. MR imaging of the liver using short TI inversion recovery sequences. J Comput Assist Tomogr. 1985; 9(6):1084–1089. [PubMed: 4056142]
35. Haase A, Frahm J, Hänicke W, Matthaei D. 1H NMR chemical shift selective (CHESS) imaging. Phys Med Biol. 1985; 30(4):341–344. [PubMed: 4001160]
36. Meyer CH, Pauly JM, Macovski A, Nishimura DG. Simultaneous spatial and spectral selective excitation. Magn Reson Med. 1990; 15(2):287–304. [PubMed: 2392053]
37. Reeder SB, Markl M, Yu H, Hellinger JC, Herfkens RJ, Pelc NJ. Cardiac CINE imaging with IDEAL water-fat separation and steady-state free precession. J Magn Reson Imaging. 2005; 22(1): 44–52. [PubMed: 15971192]
38. Reeder SB, Wen Z, Yu H, Pineda AR, Gold GE, Markl M, et al. Multicoil Dixon chemical species separation with an iterative least-squares estimation method. Magn Reson Med. 2004; 51(1):35–45. [PubMed: 14705043]
39. Ma J. Dixon techniques for water and fat imaging. J Magn Reson Imaging. 2008; 28(3):543–558. [PubMed: 18777528]
40. Hines CDG, Agni R, Roen C, Rowland I, Hernando D, Bultman E, et al. Validation of MRI biomarkers of hepatic steatosis in the presence of iron overload in the ob/ob mouse. J Magn Reson Imaging.
41. Hines, CDG.; Roen, C.; Hernando, D.; Reeder, SB. Effects of Fat Particle Size on R2* in Fat-Water-SPIO Emulsion Phantoms: Implications for Fat Quantification with Phantoms. Proceedings of 19th Annual Meeting of ISMRM; Montreal, Canada. 2011. p. 4514

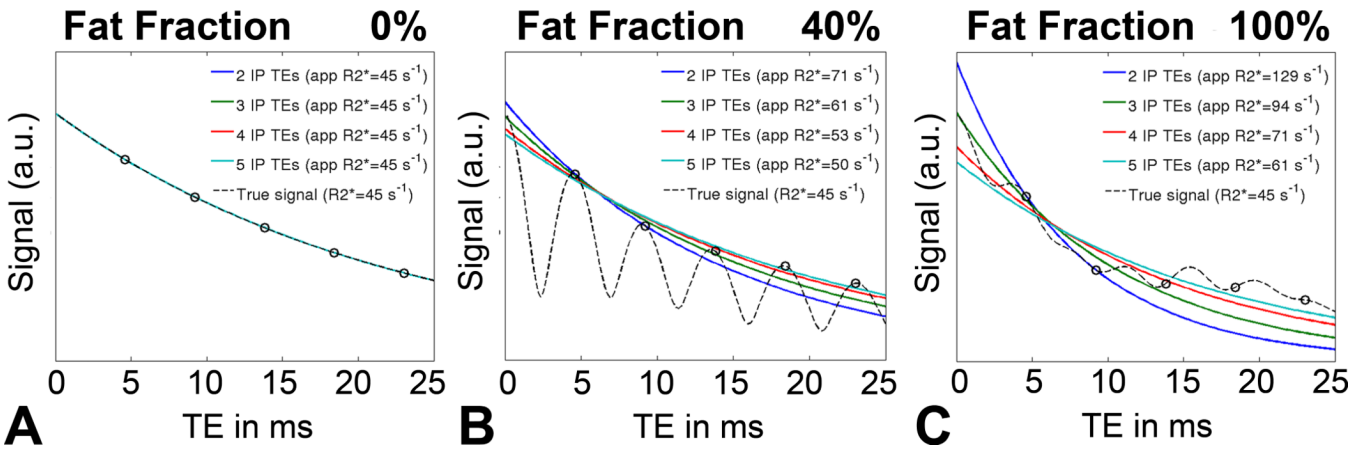

Figure 1.

Simulations demonstrate that the apparent R2* is highly dependent on the number of echoes, particularly at high concentrations of fat. The true R2* in this noiseless simulation is $45s^{-1}$. A) In cases with no fat, no errors in the apparent R2* are observed, because the ^{1}H spectrum of water has only one peak. B) In contrast, the spectrum of fat contains multiple peaks and using in-phase echoes for R2* estimation resulted in errors because of only approximately 70% of the fat signal (its main methylene peak) is truly in-phase with water at these echo times. The spectral complexity of fat results in additional oscillations that lead to errors in the apparent R2* if the spectral complexity of fat is not considered C) R2* errors increase with increasing tissue fat content.

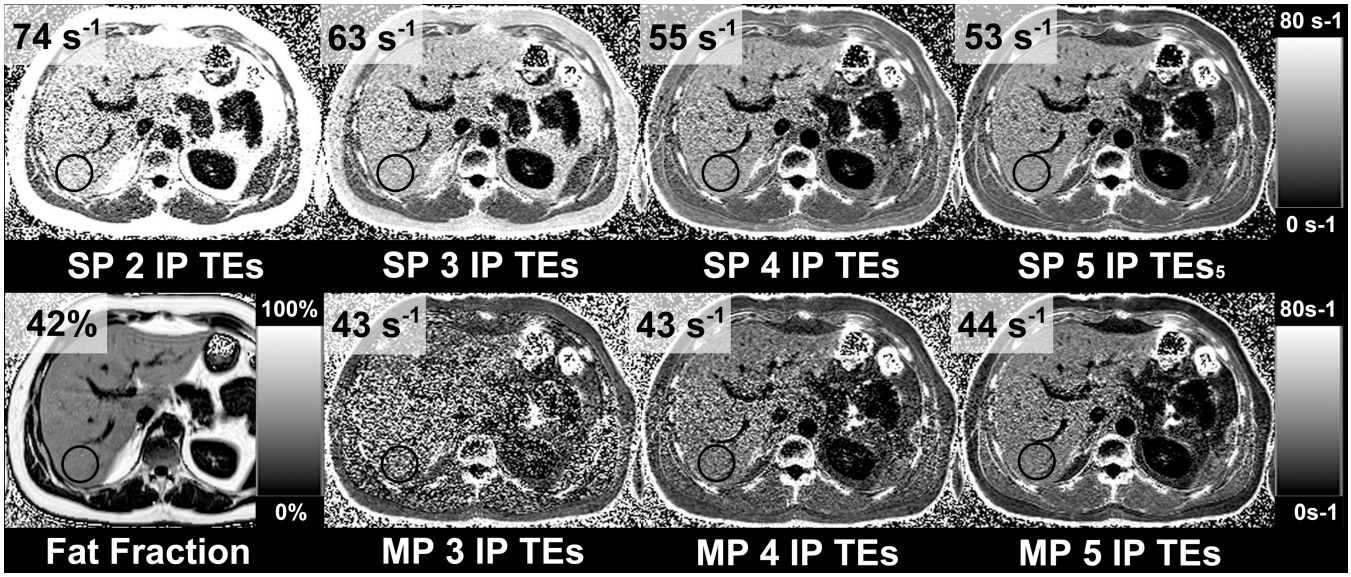

Figure 2.

The apparent R2* in the liver is highly dependent on the number of echoes if it is assumed that fat has a single-peak, even if "in-phase" echoes are used, when there is fat in the liver. The same observation is noted in subcutaneous fat, with even larger change in the apparent R2*. In this example the subject is a 34 year old man with BMI = 30.7 kg/m^2 and MRI determined liver fat-fraction of 42%. R2* maps were retrospectively reconstructed from varying subsets of echo times (out of five total in-phase echoes), using both single-peak and multi-peak fat models. In cases without multi-fat peak correction (upper row) fat increases the apparent R2*. The effects of fat on R2* can be reduced by using more echoes for the R2* estimation. However, multi-peak fat spectral modeling (bottom row) is necessary for fully fat-corrected R2* mapping.

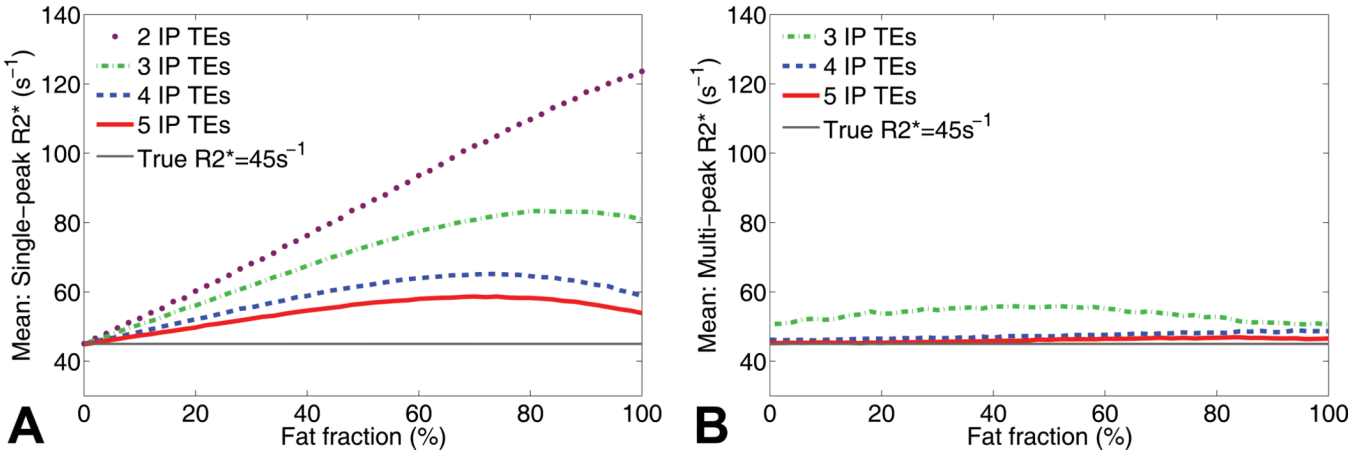

Figure 3.

Simulations show that single-peak R2* reconstructions in the presence of fat result in a severe dependence on echo combination and fat-fraction. These simulations demonstrate the dependence on the number of acquired in-phase echoes, without and with spectral modeling of fat. The true R2* in this simulation is 45 s^{-1} and Gaussian noise was added with an SNR of 30 on the first echo. A) Large errors in R2* are seen with increasing amount of fat using conventional R2* mapping without multi-peak fat modeling. The errors can be reduced with more echoes, but the effects cannot be completely corrected. B) In contrast, using multi-spectral fat modeling using 4 or more echoes, the errors in R2* in the presence of fat are corrected. R2* reconstructions using multi-peak fat modeling from 3 echoes resulted in moderate fat independent R2* estimation errors related to poor noise performance (see example in figure 2: MP 3IP TEs).

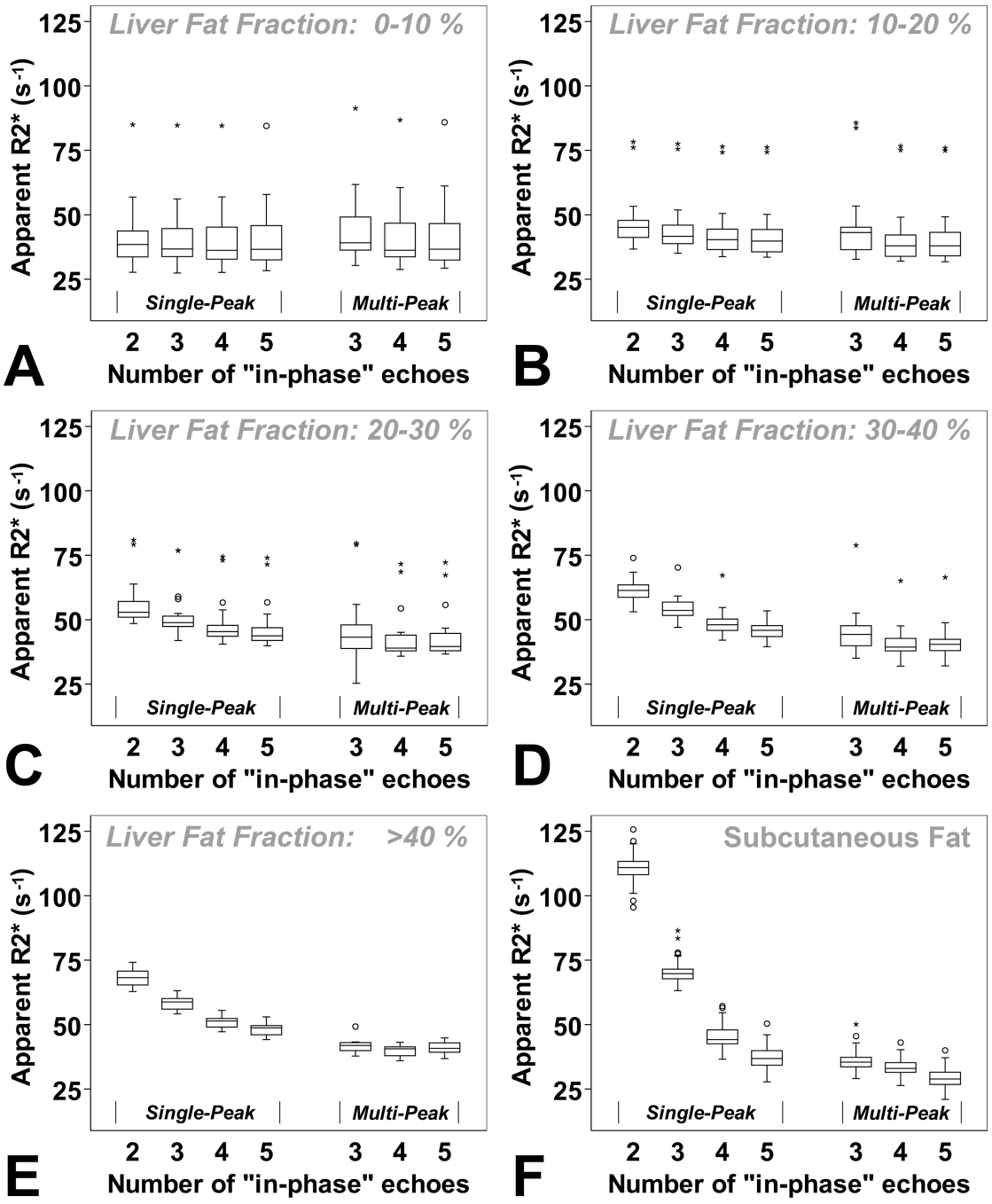

Figure 4.

Results from the 88 subjects grouped according to their liver fat-fraction determined by MRI (A: 0 – < 10%, B: 10 – < 20%, C: 20 – < 30%, D: 30 – < 40%, E: larger than 40%, and F: subcutaneous fat) confirm the theoretical results. R2* mapping using in-phase-technique and without multi-peak fat modeling resulted in large R2* estimation errors, particularly at high fat-fractions and in the subcutaneous fat. R2* errors in liver tissue may be clinically relevant for liver fat-fraction above 20–30% depending on the number of echoes used for the reconstruction. The effects of fat can be corrected using multi-peak fat modeling.

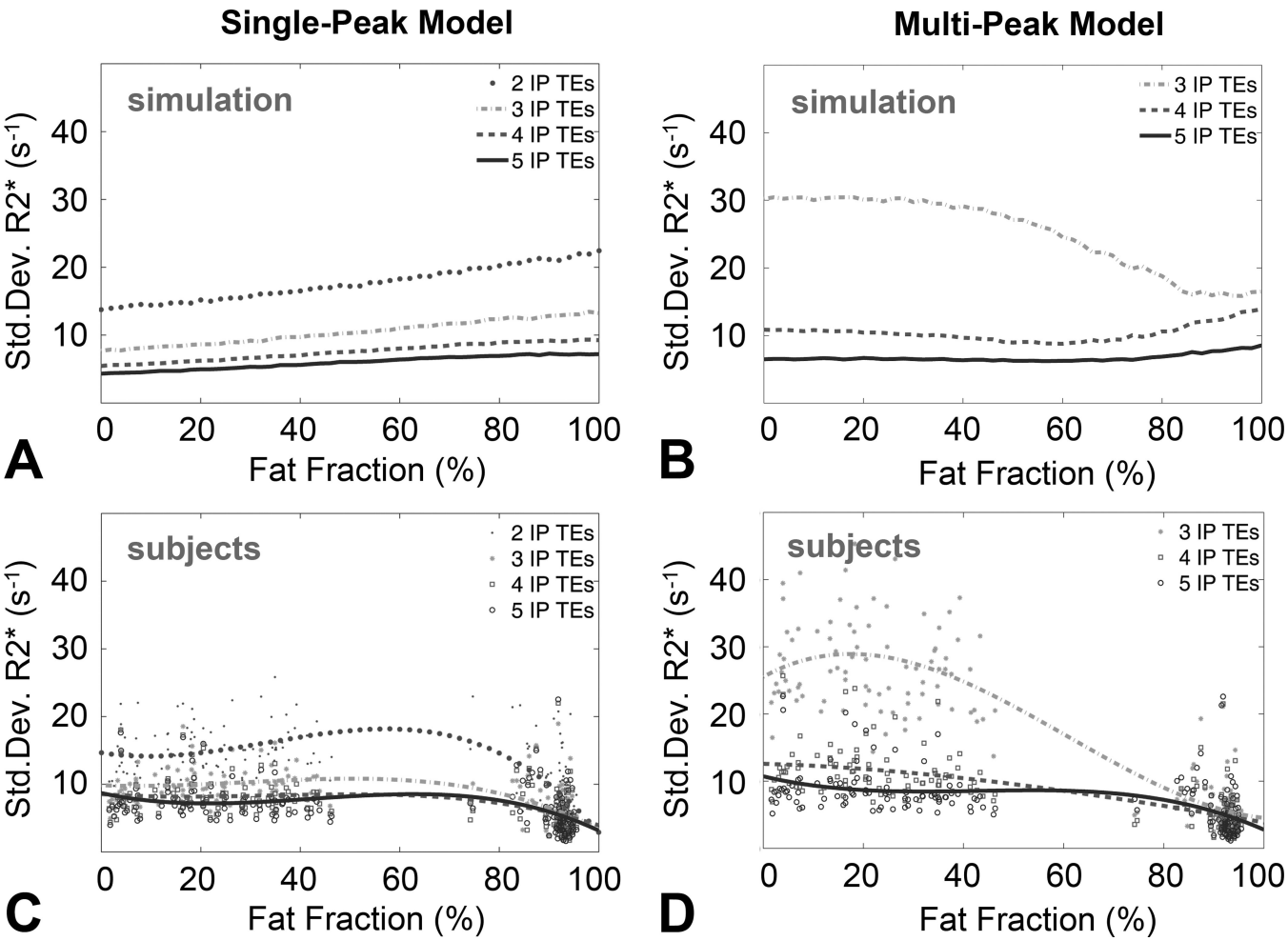

Figure 5.

Multi-peak modeling has similar noise performance to single-peak modeling, when using 4 or more echoes. The plots show standard deviation of R2* mapping from the 88 subjects, using single-peak and multi-peak reconstructions from different numbers of in-phase echoes. Simulation results (A–B, assuming a true R2* of $45 s^{-1}$) are compared to experimental results (C–D). R2* standard deviations are shown from simulations for single-peak (A), and multi-peak fat modeling (B) and for all ROIs in subjects for single peak (C) and multi-peak fat modeling (D). Thicker markers in subject results (C–D) indicate polynomial fit (3^{rd} degree) to the measured standard deviations as a function of fat-fraction. Multi-peak fat modeling resulted in poor noise performance using 3 echoes both in the simulation and in the subject data, although only a moderate increase in standard deviation relative to single-peak was observed for 4 or more echoes. It should be noted that pure fat and liver tissue have in practice different R2* values. The standard deviation of the R2* values measured in the subcutaneous tissue was low because the SNR in the tissue near the surface coils was high (C–D).

Table 1

Baseline characteristics of fat groups 1–6.

Group	subjects	PDFF ± SD (%)	Age ± SD (years)	Height ± SD (cm)	Weight ± SD (kg)	BMI ± SD (kg/m^2)
All subjects (Groups 1–5)	88	22.0 ± 12.9	55.4 ± 12.2	170.8 ± 9.7	89.8 ± 13.7	30.8 ± 3.9
Group 1	20	4.6 ± 1.9	53.7 ± 16.1	171.2 ± 8.7	83.6 ± 13.1	28.6 ± 4.4
Group 2	20	15.6 ± 2.5	55.0 ± 11.0	173.8 ± 10.9	91.6 ± 14.5	30.3 ± 3.9
Group 3	20	24.4 ± 3.5	58.5 ± 10.9	169.8 ± 9.9	91.6 ± 13.9	31.6 ± 2.5
Group 4	20	34.9 ± 2.5	58.1 ± 9.0	166.5 ± 7.5	91.1 ± 13.4	32.8 ± 4.1
Group 5	8	44.0 ± 1.9	46.4 ± 11.0	174.0 ± 11.1	93.6 ± 11.6	30.9 ± 2.7
Group 6 (adipose)	88	91.5 ± 3.8				

Baseline characteristics of fat-groups 1–6, consistent of mean proton-density liver fat fraction (PDFF) (group 1–5) and fat fraction of subcutaneous fat (group 6) ± SD (standard deviation), age, body height ± SD, body weight ± SD, and body mass index (BMI) ± SD. Subjects were randomly selected from the ongoing population-based Study of Health in Pomerania according to their liver fat content determined by MRI (group 1–5).

Table 2

R2* measurements using varying numbers of in-phase echoes.

	R2* ± SD 2 IP TEs	R2* ± SD 3 IP TEs	R2* ± SD 4 IP TEs	R2* ± SD 5 IP TEs	R2* ± SD 3 IP TEs	R2* ± SD 4 IP TEs	R2* ± SD 5 IP TEs
		Single-peak reconstruction			**Multi-peak reconstruction**		
				LIVER			
Group 1	40.8 ± 12.4	40.2 ± 12.5	40.0 ± 12.7	40.2 ± 12.8	43.7 ± 13.8	40.7 ± 13.5	40.9 ± 13.4
Group2	47.4 ± 11.0	45.1± 11.6	43.5 ± 11.8	43.1 ± 11.9	45.8 ± 14.3	41.9 ± 12.6	42.2 ± 12.4
Group 3	56.2 ± 9.0	51.9 ± 9.4	48.4 ± 9.5	47.2 ± 9.6	46.3 ± 12.9	43.2 ± 10.1	43.9 ± 10.0
Group 4	61.6 ± 4.7	54.3 ± 4.9	48.7 ± 5.4	45.7 ± 3.6	45.7 ± 9.1	40.9 ± 6.8	41.5 ± 7.0
Group 5	68.2 ± 3.7	58.4 ± 2.9	51.1 ± 2.8	48.3 ± 2.9	42.1 ± 3.4	39.9 ± 2.4	41.0 ± 2.7
	***p* ≤ 0.001**	***p* ≤ 0.001**	***p* ≤ 0.001**	***p* ≤ 0.001**	***p* = 0.396**	***p* = 0.291**	***p* = 0.158**
				SUBCUTANEOUS FAT			
Group 6	110.7 ± 4.7	70.1 ± 4.0	45.3 ± 3.9	37.5 ± 4.1	35.8 ± 3.5	33.5 ± 2.9	29.5 ± 3.5

The apparent R2* is highly dependent on the number of echoes if single peak modeling of fat is used, when fat is in high concentration. When multiple peak modeling of fat is used the apparent R2* is independent of the amount of fat and the number of echoes. The table shows mean R2* values and their standard deviation (SD) for liver tissue (group 1–5) and for subcutaneous fat (group 6) according to the reconstruction type and number of echoes used for R2* estimation. Note that single-peak reconstructions can be performed from at least two echoes, where as multi-peak reconstructions require at least three echoes. There is no effect on R2* estimation with different numbers of echoes or reconstruction type (single vs multi-peak) when there is little or no fat in the liver. However, large differences in the apparent R2* values between PDFF groups were observed when single-peak reconstruction was used. R2* was statistically independent of the number of echoes when multi-peak reconstruction was used.

Table 3

Robustness of single-peak and multi-peak reconstructions in the presence of fat.

	R2* 2 vs 3 IP TEs	R2* 3 vs 4 IP TEs	R2* 4 vs 5 IP TEs	R2* 3 vs 4 IP TEs	R2* 4 vs 5 IP TEs
	Single-peak reconstruction			Multi-peak reconstruction	
			LIVER		
Group 1	(0.05,1.14)	(−0.23,0.67)	(−0.50,0.00)	(2.15,3.79)	(−0.60,0.34)
Group2	(1.74,2.91)	(1.24,1.95)	(0.08,0.62)	(2.66,5.16)	(−0.67,0.09)
Group 3	(3.62,5.07)	(2.92,3.96)	(0.93,1.46)	(0.94,5.19)	(−1.15,−0.17)
Group 4	(6.35,8.13)	(4.92,6.22)	(1.37,4.71)	(3.39,6.22)	(−0.90,−0.19)
Group 5	(8.96,10.63)	(6.62,8.08)	(2.24,3.36)	(−0.67,5.13)	(−1.80,−0.36)
			SUBCUTANEOUS FAT		
Group 6	(39.72,41.37)	(24.27,25.34)	(7.47,8.21)	(2.01,2.77)	(3.51,4.36)

Multi-peak fat modeling results in improved robustness (smaller differences between reconstructions from different echo combinations for each subject) in the presence of fat. The table shows confidence intervals (95%) of differences between paired R2* measurements using different numbers of echoes with single-peak and multi-peak fat modeling, for each of the 6 fat-fraction groups. In the higher fat-fraction groups, smaller differences are observed using multi-peak compared to single-peak fat model.